Journal of Neuroinflammation

RESEARCH

Open Access

Minocycline prevents early age-related cognitive decline in a mouse model of intellectual disability caused by ZBTB18/RP58 haploinsufficiency

Tomoko Tanaka[1,2*], Shinobu Hirai[1], Hiroyuki Manabe[3], Kentaro Endo[4], Hiroko Shimbo[1], Yasumasa Nishito[4], Junjiro Horiuchi[4], Hikari Yoshitane[2] and Haruo Okado[1*]

Abstract

Haploinsufficiency of the transcriptional repressor ZBTB18/RP58 is associated with intellectual disability. However, the mechanisms causing this disability are unknown, and preventative measures and treatments are not available. Here, we assessed multiple behaviors in *Zbtb18/Rp58* heterozygous-knockout mice, and examined local field potentials, DNA fragmentation, mitochondrial morphology, and performed histochemical and transcriptome analyses in the hippocampus to evaluate chronic inflammation. In wild-type mice, object location memory was present at a similar level at 2 and 4–5 months of age, and became impaired at 12–18 months. In contrast, *Zbtb18/Rp58* heterozygous-knockout mice displayed early onset impairments in object location memory by 4–5 months of age. These mice also exhibited earlier accumulation of DNA and mitochondrial damage, and activated microglia in the dentate gyrus, which are associated with defective DNA repair. Notably, chronic minocycline therapy, which has neuroprotective and anti-inflammatory effects, attenuated age-related phenotypes, including accumulation of DNA damage, increased microglial activation, and impairment of object location memory. Our results suggest that Zbtb18/Rp58 activity is required for DNA repair and its reduction results in DNA and mitochondrial damage, increased activation of microglia, and inflammation, leading to accelerated declines in cognitive functions. Minocycline has potential as a therapeutic agent for the treatment of ZBTB18/RP58 haploinsufficiency-associated cognitive dysfunction.

Keywords Intellectual disability, Cognitive decline, DNA damage, DNA repair, Inflammation, ZBTB18/RP58

Introduction

Intellectual disability (ID) is a neurodevelopmental disorder in which deficits in intellectual and adaptive function begin during development [1]. Approximately 1% of the general population has ID. ID can be caused by various environmental factors, including traumas and neurological, nutritional, and metabolic disorders. Genetic factors are also major contributors to ID [2]. The 1q43q44 deletion syndrome causes ID, and the Zinc finger and BTB domain-containing protein 18 (*ZBTB18/ZNF238/ZFP238/RP58,* hereafter referred to as *RP58*) has been identified as one of the genes

*Correspondence:
Tomoko Tanaka
tanaka-tm@igakuken.or.jp
Haruo Okado
okado-hr@igakuken.or.jp
[1] Department of Psychiatry and Behavioral Science, Tokyo Metropolitan Institute of Medical Science, Tokyo 156-8506, Japan
[2] Department of Basic Medical Science, Tokyo Metropolitan Institute of Medical Science, Tokyo 156-8506, Japan
[3] Department of Neurophysiology, Nara Medical University, Nara 634-8521, Japan
[4] Center for Medical Research Cooperation, Tokyo Metropolitan Institute of Medical Science, Tokyo 156-8506, Japan

responsible for 1q43q44 deletion syndrome [3]. RP58 is a transcriptional repressor protein with a BTB domain in its N-terminus and four Zn finger motifs in its C-terminus [4]. Genome analyses of individuals with ID revealed many truncated variants [4] and nonsense and missense mutations [5, 6] in the *RP58* gene suggesting that haploinsufficiency of RP58 causes ID [7]. Thus, it is important to establish a strategy for therapy for RP58 haploinsufficiency-associated ID.

We previously generated *Rp58* conventional and conditional knockout (KO) mice and showed that RP58 plays a critical role in the formation of the cerebral cortex [7–12]. RP58 is highly expressed in the neonatal brain and its expression continues after brain maturation [13]. *Rp58* homozygous-KO mice exhibit a lethal phenotype immediately after birth, whereas *Rp58* heterozygous knockout mice (*Rp58* hetero-KO mice) are macroscopically indistinguishable from wild-type mice after birth [8]. RP58 expression continues into adulthood in the glutamatergic neurons of the cerebral cortex [13], but its postnatal role is unknown. We previously showed that *RP58* hetero-KO mice can serve as a model for human RP58 haploinsufficiency-associated ID [14]. However, it is unclear why aberrations in RP58 cause ID. Moreover, there is no known prevention or treatment strategy for this disorder.

It is well known that ID is associated with a susceptibility to dementia [55]. In this study, we focused on cognitive dysfunction in ID during adulthood using *Rp58* hetero-KO mice. Interestingly, *Rp58* hetero-KO mice showed an acceleration in age-associated impairment in spatial cognition, suggesting that these mice may serve as a model for early onset dementia associated with ID. We also observed that *Rp58* hetero-KO mice exhibit early accumulation of DNA damage, defective DNA repair, and inflammation, suggesting that the age-related cognitive impairment associated with RP58 haploinsufficiency is caused by neuroinflammation associated with defective DNA repair. The central nervous system is particularly susceptible to DNA damage repair defects, leading to various neurodevelopmental and neurodegenerative disorders, including ID [15]. Damaged DNA drives activation of the cGAS-STING signaling pathway, which induces immune responses [16]. Thus, treatments targeting DNA damage and inflammation may be effective for pathologies associated with RP58 haploinsufficiency. Interestingly, we found that minocycline, which has neuroprotective and anti-inflammatory effects [17, 18], attenuated the premature age-related phenotypes of *Rp58* hetero-KO mice, suggesting that it could form the basis of a strategy for the development of therapies of RP58 haploinsufficiency-associated cognitive dysfunction.

Materials and methods

All experimental procedures were approved by the Animal Experimentation Ethics Committee of the Tokyo Metropolitan Institute of Medical Science (49,040).

Experimental model

Animals

Rp58 KO mice, established in a C57/BL6 background, have been previously described [8]. *Rp58* hetero-KO (RP58 + / −) and C57/BL6 (RP58 + / +) mice, used in this study, were maintained under a 12:12 h light/dark cycle (lights on at 8:00 AM). Efforts were made to minimize the number and suffering of animals used, in accordance with the Animal Welfare and Control Law of Japan. Experiments were performed on young adult (2 months old), adult (4–5 months old), and old age (12–18 months old) animals (Fig. 1A). To rule out the effects of the menstrual cycle [19–21], behavioral assessments were performed using male mice.

Behavioral assessments

Male mice were habituated to a behavioral room for at least 1 h prior to the start of behavioral tests. Mice that displayed outlier behavior greater than two standard deviations from the mean were not included in behavioral analyses (3–10 in each group).

The object location test consisted of three phases as described previously [22]. All phases were performed under a light intensity of 10 lx. On day 1, the animals were placed in an empty square box (50 × 50 cm^2) for 10 min. On day 2, the animals were placed in the same box for 10 min with two identical, unfamiliar, objects. The time the animal spent exploring each object was measured automatically using a DVTrack video tracking system (Muromachi, Tokyo, Japan) and a discrimination index was calculated as (the time the animal spent exploring the object 1)—(the time the animal spent exploring the object 2)/ (the time the animal spent exploring both objects) during a 10 min testing trial. On day 3, the animals were placed in the same box, in which object 1 was displaced to a novel location, and a discrimination index was again calculated. A Δ discrimination index, which reflects the increase in time that an animal spends exploring the displaced object compared to the unmoved object was calculated by subtracting the day 3 discrimination index from the day 2 discrimination index.

For the open field test, each mouse was placed in the center of the apparatus (50 × 50 cm^2) and was allowed to move freely for 30 min under a light intensity of 10 lx. Horizontal activity was collected every 10 min using the

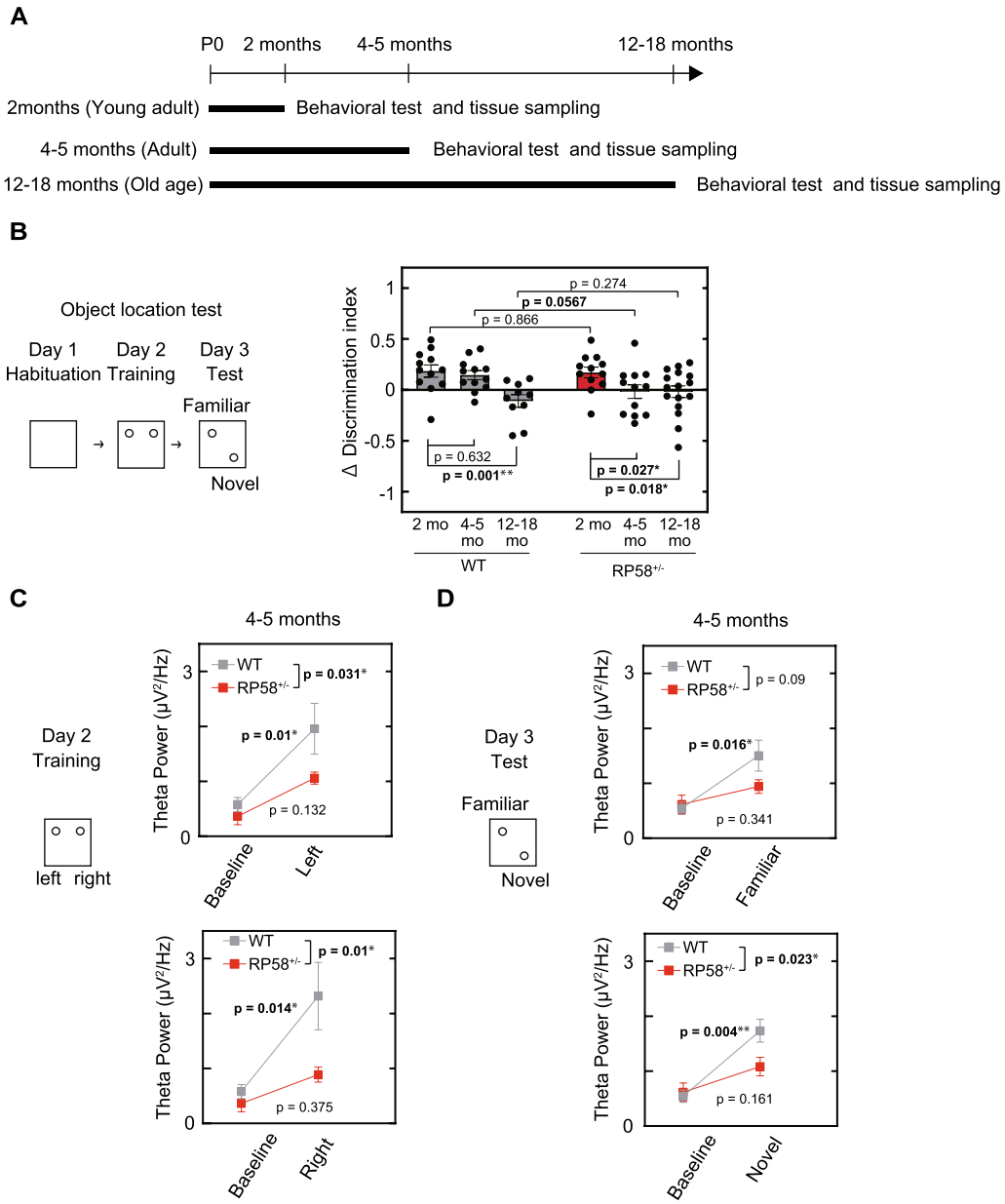

Fig. 1 Spatial memory and hippocampal function in *Rp58* hetero-KO mice. **A** Experimental schedule. **B** Object location memory in wild-type and *Rp58* hetero-KO mice at different ages. One of two familiar objects was moved on day 3 and change in time spent exploring the object in the new location (Δ discrimination index) was measured (see Materials and Methods for details). *$p < 0.05$, **$p<0.01$; $n = 12$ for both genotypes at 2- or 4–5-months of age, $n = 10$ for 12–18-month-old wild-type mice, and $n = 16$ for 12–18-month-old *Rp58* hetero-KO mice. **C** Theta power in the hippocampal CA1 region of 4–5-month-old wild-type- and age-matched *Rp58* hetero-KO mice on day 2 and day 3 of the object location test. *$p < 0.05$, **$p < 0.01$; $n = 5$ for each genotype

DVTrack video tracking system (Muromachi, Tokyo, Japan).

The rotarod test consisted of five trials with 1 h intervals between trials. Prior to testing, to habituate the mice to the rotarod, the animals were placed for five minutes on the rotarod (3 cm diameter; MK-660B; Muromachi Kikai Co., Ltd., Tokyo, Japan) that was rotating at 1 and 4 rpm. During testing, to assess motor learning ability, the rotarod was accelerated from 1–40 rpm over a period of five minutes.

The fear conditioning test consisted of three phases as described previously [22]. On day one, animals were placed in a triangular box for 5 min under a light intensity of 30 l×. On day 2, the animals were placed in a square

box with a stainless-steel grid floor with a light intensity of 100 l× and were allowed to explore the box freely for 2 min. Subsequently, a tone, which served as the conditioned stimulus (CS), was presented for 30 s. During the last 1 s of the presentation of the CS, a 0.75 mA electric shock was applied, which served as the unconditioning stimulus (US). Two more CS-US pairings were presented with a 1-min inter-stimulus interval. On day 3, the animals were placed in the same box used on day 2 for 5 min under a light intensity of 100 lx and the percent freezing time and distance traveled (cm) were calculated automatically using ImageFZ software (O'Hara & Co., Tokyo, Japan).

Electrophysiology

Mice were anesthetized with isoflurane (1.5%) and a custom-designed electrode consisting of two tetrodes was implanted in the CA1 area of the hippocampus (1.8 mm anterior to bregma, 1.4 mm lateral to the midline, and 1.2 mm from the brain surface). Individual tetrodes consisted of four twisted polyimide-coated tungsten wires (single wire diameter, 12.7 μm; California Fine Wire, Grover Beach, CA). A screw was threaded into the bone above the cerebellum as a reference and for grounding. The electrodes were connected to an electrode interface board (EIB-18, Neuralynx, MT) on a microdrive. Mice were allowed to recover from surgery for at least one week before behavioral assessments.

Local field potential (LFP) recordings were obtained at a sampling rate of 30 kHz using open-source hardware (Open Ephys, Cambridge, MA) while mice were engaged in the object location test. For synchronization with behavioral data, a transistor-transistor logic pulse was used. After recordings, electrode lesions were induced with direct current (20 μA) stimulation for 10 s using one of the four tetrode leads.

Analysis of electrophysiology data

All data analyses were performed using the built-in software in MATLAB (MathWorks, Inc., MA). LFPs were down-sampled to 1,000 Hz and the data from 1 s before to 1 s after contact with the objects were extracted. Theta power was calculated as the mean value of the power spectrum between 4 and 8 Hz. This value was normalized to the theta power of mice during walking.

Immunohistochemistry

Young adult, adult, and old age male and female mice were anesthetized with isoflurane, and sequentially transcardially perfused with phosphate-buffered saline (PBS) and 4% paraformaldehyde (PFA) in PBS. Brains were removed, post-fixed, cryoprotected in 20% sucrose overnight and then in 30% sucrose for two days at 4 °C, embedded in optimal cutting temperature compound, and frozen at − 30 °C. 20 μm coronal sections were obtained using a cryostat. Free-floating sections containing the hippocampus were incubated in HistoVT One (Nakalai, Kyoto, Japan) at 70 °C for 20 min, incubated in 0.4% Block Ace diluted in PBS containing 0.2% Triton X-100 (DS Pharma Biomedical, Osaka, Japan) in PBS at room temperature (RT) for 20 min, and then incubated with primary antibodies (Supplemental Table 1). Primary antibodies were diluted 1:500 in PBS containing 0.3% Triton X-100. Sections were then incubated with secondary antibodies (Jackson, ME) diluted 1:500 in PBS containing 0.3% Triton X-100.

For GluR2, Rp58, and parvalbumin (PV) triple staining, 50 μm tissue sections were incubated at RT for 20 min in 1% H_2O_2 after incubation with HistoVT One. After further incubation in PBS containing 1% Block Ace and 0.2% Triton X-100, sections were incubated with rabbit anti-GluR2 (1:500), chicken anti-RP58 (1:1000), and goat anti-PV antibody (diluted 1:1000 in PBS containing 0.4% Block Ace) and then incubated with secondary antibody (diluted 1:1000 in PBS). To enhance the GluR2 signal, a biotinylated anti-rabbit secondary antibody was used, and the biotin was labeled with horseradish peroxidase (HRP) using the VECTASTAIN Elite ABC-HRP Kit (Vector #PK-6100). GluR2 was detected using Tyramide Signal Amplification (TSA) Cyanine 3 (Perkin Elmer #FP1046). Tissue sections were incubated with DAPI (Nacalai Tesque, Kyoto, Japan) for nuclear staining. Micrographs of immunofluorescence-stained sections were captured and digitized using a FluoView® FV3000 confocal laser scanning microscope (Olympus, Tokyo, Japan).

Analysis of immunostaining

To quantify single-stranded DNA (ssDNA) and gamma H2AX in cells, the number of cells with five or more nuclear ssDNA foci or gamma H2AX foci was counted [23]. For the analysis of microglia states, immunostaining with an antibody against CD68 was performed. CD68 is a lysosomal-associated protein found in macrophages/microglia and is associated with phagocytic cells. An Iba1 antibody was used as a marker for both resting and activated microglia. Microglia with aggregated CD68 expression were categorized as reactive, and the percentage of reactive microglia was compared between groups [24, 25]. Antibody information is provided in the Key Resources table.

Irradiation

Animals were irradiated with a dose of 0.3 Gy. At 1-, 6-, or 24 h after irradiation, mice were anesthetized with isoflurane and transcardially perfused with PBS followed by

4% PFA in PBS. Subsequent steps were described earlier under immunohistochemistry.

Electron microscopy

Adult male and female mice were anesthetized with isoflurane and transcardially perfused with saline followed by 2% PFA and 2.5% glutaraldehyde in 0.1 mol/L phosphate buffer (pH 7.4). Brains were removed, post-fixed, and coronal sections containing the dentate gyrus were obtained using a VT1200S microtome (300 μm) (Leica, Wetzlar, Germany). Micro-dissected areas were post-fixed for 2 h at 4 °C in 2% osmium tetroxide in 0.1 mol/L cacodylate buffer. Tissue blocks were dehydrated sequentially in 50% ethanol for 5 min, 70% ethanol for 15 min, 80% ethanol for 15 min, 90% ethanol for 15 min, and in 100% ethanol at RT for 20 min. Tissues were then infiltrated with propylene oxide three times for 10 min each, treated with a 1:1 solution of propylene oxide:epoxy resin for 2 h, and incubated in epoxy resin overnight. Each block was placed flat on glass microscope slides and horizontally mounted on gelatin capsules (Lilly, IN). After embedding, each block was polymerized in epoxy resin (EPON 812, TAAB, Berkshire, England) at 60 °C for 48 h. Polymerized blocks were trimmed to a section containing the dentate gyrus using an ultramicrotome PowerTomeX (RMC Boeckeler, AZ). 1 μm semi-thin sections were stained with toluidine blue and used to guide further cutting of the specimen block to ultra-thin Sects. (50–80 nm). Ultra-thin sections were placed in formvar-coated single-slot grids. After staining with uranyl acetate and lead citrate, sections were observed under a JEM-1400 transmission electron microscope (JEOL, Tokyo, Japan) equipped with a bottom-mounted charge-coupled device camera and subsequently processed using ImageJ.

Quantification of ultrastructural defects: Quantification of mitochondrial ultrastructural defects was performed on transmission electron microscopy images acquired at a magnification of 10,000×. Although mitochondria are sparse within astrocytic processes of the dentate gyrus, the criteria used by Sisková et al. [26] for the identification of astrocytes and neuronal cells were applied to ensure that neuronal mitochondria were observed. Every mitochondrion of neuronal origin was analyzed and, based on its ultrastructural appearance, classified into one of the following categories according to Sisková et al. [27]. At least 14 mitochondria from each region were analyzed per animal.

Drug treatment

Minocycline was administered in drinking water to wild-type and *Rp58* hetero-KO mice from weaning to the day before the behavioral test or perfusion. Minocycline was dissolved at a concentration of 0.015 mg/mL in filtered water.

Maicroarray analysis

Three independent total RNA samples from hippocampi of mice in each group were purified using a RNeasy Plus Universal Kit (Qiagen, Hilden, Germany). RNA quality was assessed using a 2100 Bioanalyzer (Agilent Technologies, Santa Clara, CA). Cy3-labeled complementary RNA was prepared using a Low Input Quick Amp Labeling Kit (Agilent Technologies) in accordance with the manufacturer's protocol. Samples were hybridized to the SurePrint G3 Mouse Gene Expression v2 Microarray (G4852B; Agilent Technologies). Thereafter, the array was washed and scanned using the SureScan Microarray Scanner (Agilent Technologies). Microarray images were analyzed using Agilent's Feature Extraction software (Agilent Technologies) with default settings for all parameters. Data from each microarray analysis were normalized by shifting to the 75th percentile without baseline transformation. Microarray results were deposited in the Gene Expression Omnibus database under the accession number GSE207955.

Statistical analysis

Group data are presented as the means ± SEMs. The statistical significance of Δ discrimination index scores and total horizontal activities were assessed using two-way ANOVA followed by uncorrected Fisher's LSD for object location tests, two-way ANOVA followed by uncorrected Fisher's LSD were used for theta power in the hippocampal CA1 region, immunostaining experiment for minocycline treatment, two-way repeated ANOVA was used for open field, rotarod, and fear conditioning tests, Student's t-tests were used for immunostaining experiments other than minocycline treatment, Pearson's chi-squared tests were used for electron microscopy. Statistics were calculated using Prism (GraphPad Software, MA).

Results

Rp58 heterozygous-KO mice exhibit early-onset cognitive decline

We investigated whether *Rp58* hetero-KO mice had behavioral deficits by conducting multiple tests. They exhibited impairments in object location tests at 4-5 months of age (Fig. 1B), suggesting a defect in spatial learning. We investigated whether this spatial learning defect was age-dependent. Mice at 2-, 4–5, and 12–18-months of age were used as young adult, adult, and old age mice, respectively. Wild-type mice at 2 months of age spent more time exploring a familiar object in a novel location to one at a familiar location, as demonstrated by a positive Δ discrimination index.

The Δ discrimination index in 4–5-month-old wild-type mice was similar to that in mice at 2 months of age, while the Δ discrimination index at 12–18-months of age was significantly lower, indicating an age-dependent impairment in spatial learning or memory (Fig. 1B). *Rp58* hetero-KO mice exhibited the same level of object location memory as wild-type mice at 2-months of age. However, at 4–5-months of age, the Δ discrimination index was significantly reduced, indicating early-onset cognitive impairment. None of the mice used in the object location test showed significant differences in distance travelled (Supplemental Fig. 1-A), indicating that there is no difference in locomotor performance between wild-type and *Rp58* hetero-KO mice. Since *Rp58* hetero-KO mice at 4–5 months of age did not show significant behavioral effects in other behavioral tests: open field, rotarod, and fear conditioning tests (Supplementary Fig. 1-B, C, D), spatial learning seems to be specifically impaired in *Rp58* hetero-KO.

The hippocampal CA1 region is crucial for spatial learning and theta power is associated specifically with the encoding of new information [28]. Thus, we next recorded the theta power in the CA1 region of the hippocampus (Fig. 1C). In 4–5-month-old wild-type mice, average theta power level increased significantly compared to baseline in a time window encompassing one second before to one second after contact with an object. This increase was observed both when animals were first introduced to the objects on day two, and when animals were reintroduced to the objects on day 3. In 4–5-month-old *Rp58* hetero-KO mice, the theta power increase was not only attenuated on day 3, but was already significantly attenuated on day 2 compared to wild-type. These results demonstrate that the object recognition defects in *Rp58* hetero-KO mice are correlated with decreased theta power and may be caused by a defect in learning the location of an object rather than in memory recall.

Rp58 heterozygous-KO mice show early accumulation of DNA damage in mossy cells of the dentate gyrus

Spatial learning is dependent on hippocampal function. To identify the cells in the hippocampus that contribute to the deficits in spatial memory in *Rp58* hetero-KO mice, we examined the localization of RP58 protein in the hippocampus. Consistent with previous work [14], RP58 was expressed in CA1-CA3 pyramidal cells and dentate gyrus granule cells. Furthermore, in the hilus of the dentate gyrus, we found that RP58 was highly expressed in GluR2 (glutamate ionotropic receptor AMPA type subunit 2)-positive mossy cells [29], but not in PV-positive GABAergic neurons (Fig. 2A). Thus, RP58 is expressed not only in CA1-3 pyramidal neurons of the hippocampus and granule cells of the granular layer, but also in mossy cells of the hilus region. The expression of RP58 in these neurons prompted us to investigate the possibility that early cognitive decline is caused by damage to these neurons in *Rp58* hetero-KO mice. RP58 has been proposed to protect against DNA damage and contribute to cell survival [8]. Thus, we examined the presence of ssDNA, a marker of DNA damage, in hippocampal neurons, and detected ssDNA immunoreactivity in the nuclei and cytosol of many mossy cells. DNA normally resides in the nucleus and mitochondria, so its presence in the cytoplasm serves as a danger-associated molecular pattern [30]. Mossy cells play a crucial role in spatial memory by receiving convergent excitation from granule cells and returning bilateral, widespread, and divergent excitatory outputs to granule cells [31, 32]. In wild-type mice, the number of ssDNA-positive neurons gradually increased from 2-months of age to 12–18-months of age (Fig. 2B). 2-month old *Rp58* hetero-KO and wild-type mice had similar numbers of ssDNA-positive neuron, but at 4–5 months of age, the number of ssDNA-positive neurons in *Rp58* hetero-KO mice significantly increased compared to age-matched control. This demonstrates that *Rp58* hetero-KO mice show an acceleration of DNA

(See figure on next page.)

Fig. 2 Cellular mechanisms of DNA damage in *Rp58* hetero-KO mice. **A** Localization of RP58 protein in the hippocampal formation in adult mice. Triple staining for RP58, GluR2, and PV indicates that RP58 is expressed in pyramidal cells of hippocampal CA1-CA3, granular neurons, and hilar mossy cells (indicated by arrowheads) of the dentate gyrus, but not in PV-positive GABAergic neurons (indicated by arrows). Scale bar (left) = 200 µm; scale bar (right) = 50 µm. **B** Accumulation of ssDNA (indicated by arrows) as a marker of DNA damage in neurons in the dentate gyrus of wild-type- and *Rp58* hetero-KO mice. *$p < 0.05$; $n = 3$ for both genotypes at 2- or 12–18 months of age, and $n = 4$ for both genotypes at 4–5 months of age. scale bar = 20 µm. **C** Accumulation of gamma-H2AX protein (indicated by arrows) as a marker of DNA damage in neurons in the dentate gyrus of wild-type and *Rp58* hetero-KO mice. $n = 3$ per group. scale bar = 20 µm. **D** Microglia, detected using anti-Iba1 antibody (magenta), and activated microglia, detected using anti-CD68 antibody (cyan), in the dentate gyrus of wild-type- and *Rp58* hetero-KO mice. *$p < 0.05$; $n = 3$ for both genotypes at 2- or 12–18-months of age, and $n = 4$ for both genotypes at 4–5-months of age. scale bar in top = 20 µm, scale bar in bottom = 10 µm. **E** Morphological abnormalities of neuronal mitochondria in the dentate gyrus of wild-type- and *Rp58* hetero-KO mice. Mitochondria were classified according to their ultrastructural appearance into one of four categories as previously described [27]. Granule cell layer: chi-square = 284.837, degrees of freedom (df) = 3, $p < 0.001$; hilus: chi-square = 359.525, df = 3, ***$p < 0.001$; $n = 3$ per group. scale bar in right = 0.2 µm

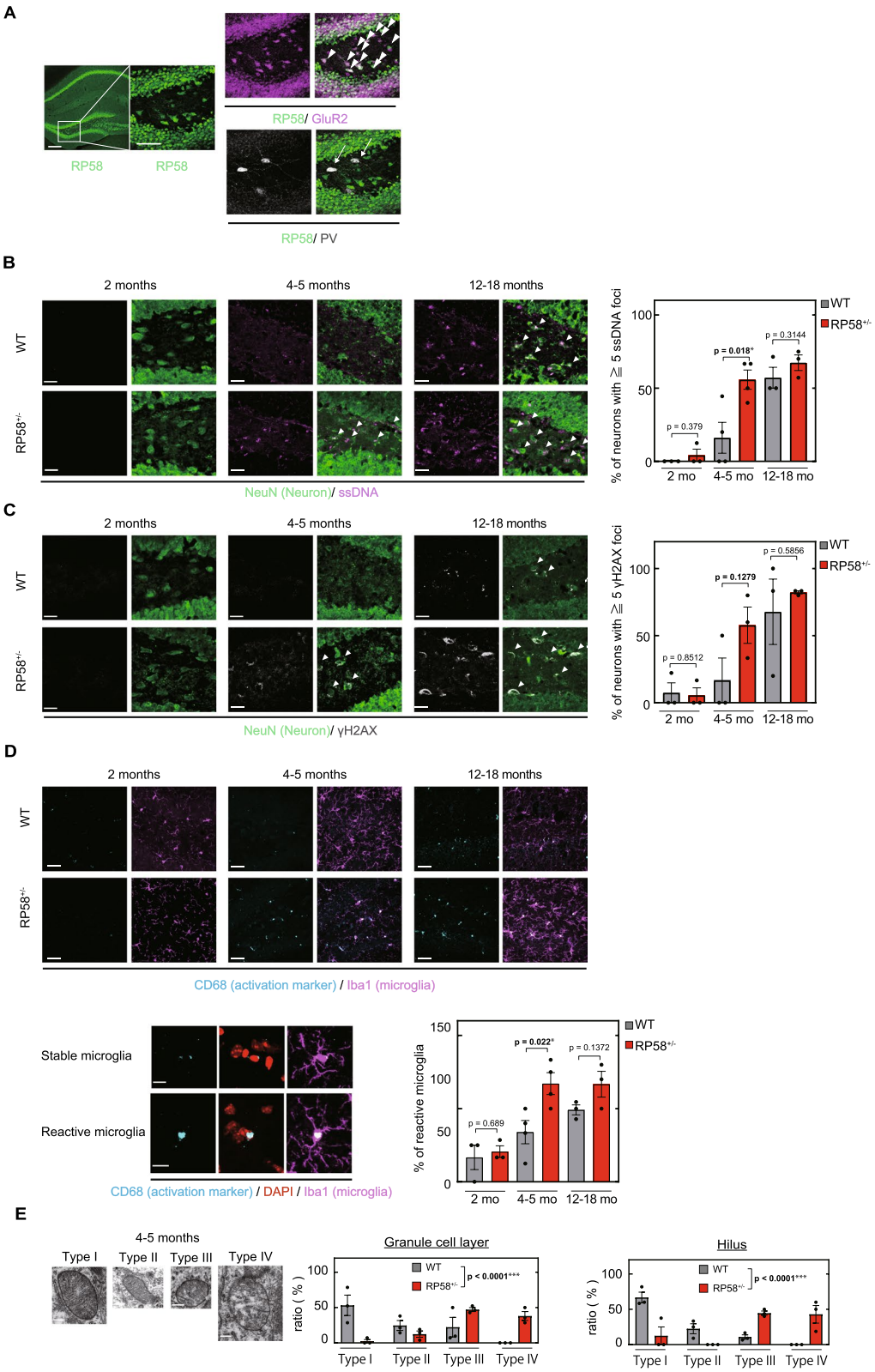

Fig. 2 (See legend on previous page.)

damage accumulation in mossy cells compared to wild-type. Early accumulation of DNA damage in heterozygous mice was further confirmed using another marker of DNA damage, gamma-H2AX, a form of H2AX protein phosphorylated at Ser139 [33] (Fig. 2C). Cytoplasmic H2AX has been reported to be important for cell death upon DNA damage [34], suggesting that RP58 may be important in preventing the accumulation of DNA damage and cell death in mossy cells in the dentate gyrus, thereby preserving spatial learning.

An increase in activated microglia and chronic inflammation in *Rp58* heterozygous-KO mice

We subsequently focused on microglia in the hilar region of the dentate gyrus because activated microglia are known to accumulate at the periphery of neurons with DNA damage [35]. We immunostained hippocampal slices with CD68 antibody to detect activated microglia and Iba1 antibody to detect total microglia. In wild-type mice, the percentage of activated microglial cells gradually increased between the ages of 2 and 12–18 months (Fig. 2D). *Rp58* hetero-KO mice had a similar percentage of activated microglia as wild-type at 2 months of age, but showed a significant increase in activated microglia at 4–5 months of age compared to age-matched controls. This early increase in activated microglia raised the possibility that chronic inflammation in the brain may be induced at earlier ages in *Rp58* hetero-KO mice. To test this possibility, we examined gene expression profiles in the hippocampus of 4 month old wild-type, 4 month old *Rp58* hetero-KO, and 12–18-months-old wild-type mice. Among 668 genes whose expression was reduced in 12–18 month old wild-type mice compared with 4–5-month-old wild-type mice, 341 were also reduced in 4–5-month-old *Rp58* hetero-KO mice. Conversely, expression of 103 genes was increased in both 4–5-month-old *Rp58* hetero-KO and aged wild-type mice when compared with 4–5-month-old wild-type mice (Supplemental Fig. 2A). Pathway enrichment analysis revealed that these 103 up-regulated genes included *Cxcl10*, *Oas2*, *Oas1a,* and *Oasl2* (Supplemental Fig. 2B), which are associated with a pathway of immune response interferon gamma action on extracellular matrix and cell differentiation (Supplemental Fig. 2C).

Ultrastructural changes in the mitochondria of *Rp58* hetero-KO mice

We also examined mitochondrial changes in *Rp58* hetero-KO mice. Mitochondria have a crucial role in antigen presentation and innate immune reactions [36, 37] and aging has been shown to increase mitochondrial abnormalities [38]. In the current study, we categorized the mitochondrial structure into four types, intact mitochondria with normal-appearing cristae (Type I), abnormal mitochondria with either swollen, irregular, or whirling cristae (Type II), mitochondria with a discontinuous outer membrane or deficient cristae (Type III), and mitochondria with both swollen and deficient cristae or with both a discontinuous outer membrane and swollen cristae (Type IV). In 4–5-month-old *Rp58* hetero-KO mice, the majority of mitochondria in neurons in the granule cell layer and in the hilar region were categorized as Types III and IV, whereas the majority of mitochondria in age-matched controls were categorized as Types I to III (Fig. 2E). It should be emphasized that Type IV mitochondria, which show (i) swollen and deficient cristae or (ii) swollen cristae and a discontinuous outer membrane, were detected only in *Rp58* hetero-KO mice (Fig. 2E).

DNA repair is impaired in *Rp58* hetero-KO mice

The accelerated accumulation of DNA damage in *Rp58* hetero-KO mice described earlier could be due to impaired DNA repair [39, 40]. Thus, we monitored the recovery of *Rp58* hetero-KO mice from irradiation-induced DNA damage (Fig. 3A). ssDNA-positive neurons were not detected in non-irradiated 2-month-old wild-type mice (Fig. 2B), but they were detected in the granule cell layer of the dentate gyrus one hour after irradiation (1 dose, 0.3 Gy) (Fig. 3B). The number of ssDNA-positive neurons gradually decreased between 1 and 24 h after irradiation in wild-type mice (Fig. 3B), demonstrating the occurrence of DNA repair. In *Rp58* hetero-KO mice, a similar extent of ssDNA accumulation was observed 1 h after irradiation. However, the percentage of neurons with ssDNA damage maintains significantly higher levels 24 h after irradiation compared to wild-type mice, indicating that DNA damage was not being repaired. This result was confirmed using another marker of DNA damage, gamma-H2AX (Fig. 3C). Moreover, while the percentage of activated microglia was high in wild-type mice 1 h after irradiation, it decreased within 24 h after irradiation. In contrast, the percentage of activated microglia was high 1 h after irradiation in *Rp58* hetero-KO mice and remained significantly higher levels for at least 24 h compared to wild-type mice (Fig. 3D). These data support the idea that RP58 activity is important for DNA repair and suppression of microglial activation. Thus, the accelerated accumulation of DNA damage in *Rp58* hetero-KO mice is likely caused by a defect in the DNA repair.

Chronic treatment with minocycline prevents early-impaired aging phenotypes in *Rp58* hetero-KO mice

Minocycline is a tetracycline antibiotic that has recently been shown to have neuroprotective [18] and anti-inflammatory effects [17] on the progression of several neurodegenerative disorders. In order to determine

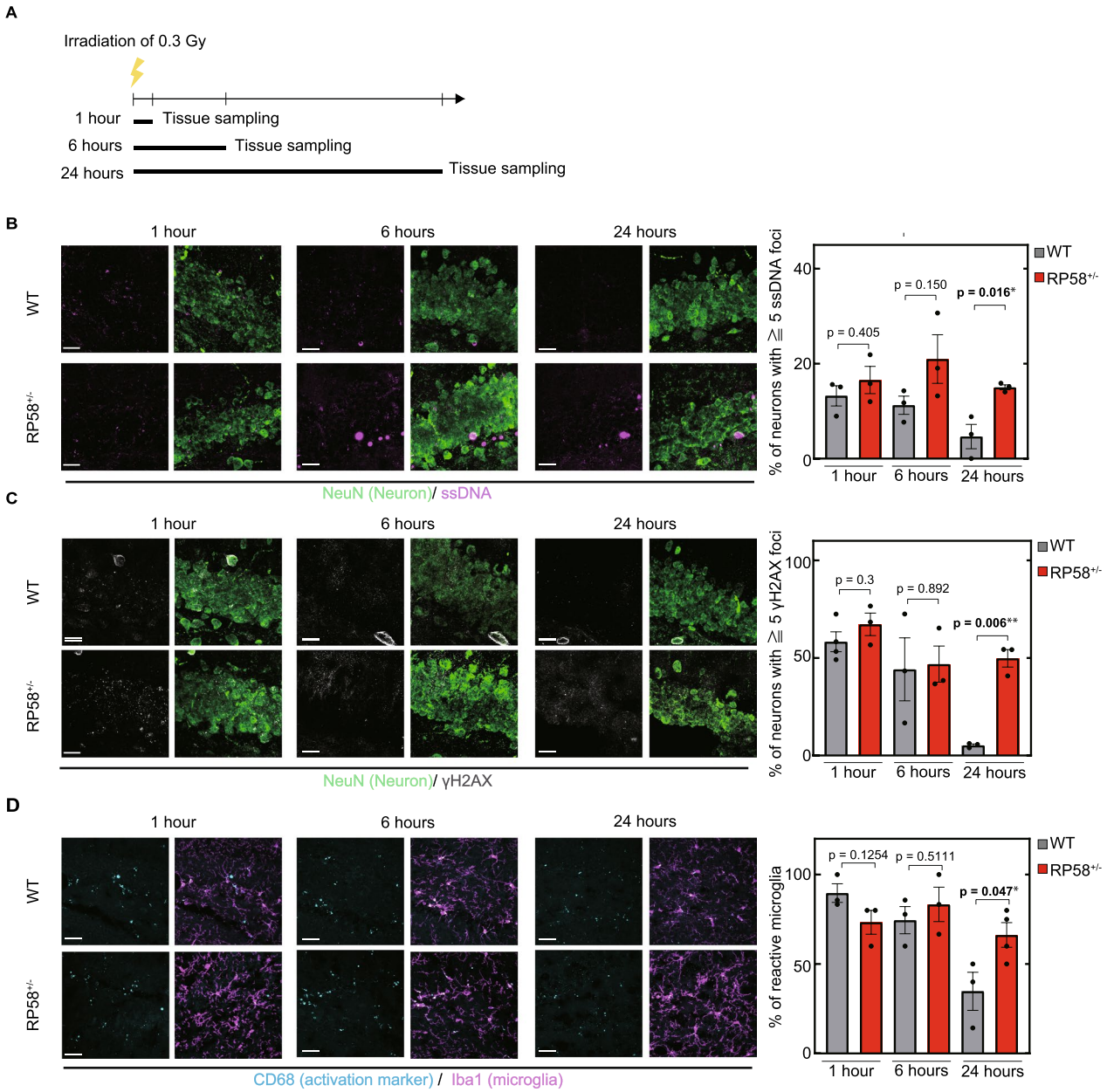

Fig. 3 DNA repair dysfunction in *Rp58* hetero-KO mice. **A** Sampling schedule after irradiation. **B** Accumulation of irradiation-induced ssDNA as a marker of DNA damage (magenta) in neurons in the dentate gyrus of wild-type and *Rp58* hetero-KO mice. *$p < 0.05$; $n = 3$ per group. scale bar = 20 µm. **C** Irradiation-induced accumulation of gamma-H2AX protein (gray) as a marker of DNA damage in neurons in the dentate gyrus of wild-type- and *Rp58* hetero-KO mice. **$p < 0.01$; $n = 3$ per group. scale bar = 20 µm. **D** Microglial activation detected by labeling microglia with Iba1 and CD68 in the dentate gyrus of wild-type- and *Rp58* hetero-KO mice. *$p < 0.05$; $n = 3$ per group. scale bar in left = 20 µm, scale bar in right = 10 µm

whether minocycline may ameliorate the DNA repair and behavioral defects of *Rp58* hetero-KO mice, we administered minocycline in the drinking water of wild-type and *Rp58* hetero-KO mice from 1 month of age to 4–5 months of age (Fig. 4A). Chronic treatment with minocycline prevented the increase of ssDNA-positive and/or gamma-H2AX-positive neurons in the dentate gyrus of 4–5-month-old *Rp58* hetero-KO mice (Fig. 4B, C). Furthermore, it prevented the early increase in activated microglia found in the dentate gyrus of *Rp58* hetero-KO mice (Fig. 4D). We also examined the effect of minocycline on the impairment of object location

memory in 4–5-month-old *Rp58* hetero-KO mice and found that it prevented cognitive dysfunction in *Rp58* hetero-KO mice (Fig. 4E). Taken together, our results suggest that RP58 is involved in DNA damage repair and its reduction induces inflammation, activation of microglia, and impaired cognitive function. They further suggest that minocycline may have potential as a therapeutic strategy for the amelioration of cognitive impairments associated with RP58 haploinsufficiency through its ability to prevent DNA damage accumulation and an increase in activated microglia.

Discussion

In this study, we analyzed *Rp58* hetero-KO mice to obtain insights into the pathogenesis of ZBTB18/RP58 haploinsufficiency-associated ID and identify preventive treatment methods. *Rp58* hetero-KO mice showed accelerated age-associated impairment of spatial cognition, accumulation of DNA damage in neurons in the hippocampal dentate gyrus hilus, and an increase in activated microglia. In the dentate gyrus hilus, RP58 was strongly expressed in mossy cells but not in PV-positive cell GABAergic neurons, suggesting that heterozygous loss of RP58 induces abnormalities in mossy cells. Physiological analyses revealed that the normal increase in theta power in the hippocampal CA1 region that occurs during object location learning is attenuated during adulthood in *Rp58* hetero-KO mice; theta power in the CA1 region is involved in dentate granule cell activity, which is regulated by mossy cell circuitry [41]. Therefore, we propose that dysfunction of mossy cells in *Rp58* hereto-KO mice contributes to the impairment of theta power in the CA1 region, leading to impaired spatial cognition. Mice with RP58 heterozygous deletions also show an accelerated accumulation of DNA damage in a group of neurons in the hippocampal dentate gyrus hilus, and these mice are deficient in DNA repair compared to wild-type mice, suggesting that RP58 insufficiency induces dysfunction in mossy cells by inhibiting DNA repair pathways.

Consistent with previous studies showing that minocycline selectively inhibits microglial activation [17, 42], our data demonstrate that minocycline inhibits microglial polarization to a proinflammatory state in *Rp58* hetero-KO mice. Microglia change from a ramified morphological state to a de-ramified spheroid structure with abnormal processes upon aging [43]. In our study, we find an increase in activated microglia in 12–18-month-old wild-type mice that is accelerated in *Rp58* hetero-KO mice and present at 4–5-months of age. While microglia protect neurons via inflammatory responses and phagocytosis in early phases of activation, they have detrimental effects at late phases. Our results suggest that the accelerated accumulation of activated microglia is detrimental to neurons in the hippocampal dentate gyrus hilus. It was recently reported that RP58 in hepatocytes regulates activity of the NLRP3 inflammasome in macrophages and inflammation in the liver [44]. Similarly, RP58 haploinsufficiency in mossy cells may cause activation of microglia via the NLRP3 inflammasome, inducing neuroinflammation and damaging neurons. Supporting this idea, minocycline has been reported to inhibit activity of the NLRP3 inflammasome [42, 45–48], suggesting that minocycline inhibits microglial activation in *Rp58* hetero-KO mice through inhibition of the NLRP3 inflammasome.

Minocycline is also known to positively regulate FOXO-dependent autophagy [50], and RP58 has been reported to cooperate with FOXO1 [49]. RP58 is a transcription factor that represses transcription of genes that represses autophagy [51]. RP58 expression decreases upon aging [52] and the resultant decrease in autophagy is thought to be one of the causes of accumulating DNA damage [53]. We propose that the reduced RP58 in *Rp58* hetero-KO mice also reduces autophagy, leading to accumulation of DNA damage in mossy cells. Damaged mossy cells release chemokines including damage-associated molecular patterns(DAMPs), which activate microglia via the NLRP3 inflammasome [16]. Thus, RP58 insufficiency may cause neuronal damage and memory defects by increasing inflammasome activity and/or decreasing autophagy. Further studies are needed to elucidate the mechanism by which RP58 regulates DNA damage repair. Altogether, our results suggest that minocycline has potential as an agent for the treatment of patients with ZBTB18/RP58 haploinsufficiency. Minocycline is already used as a treatment

(See figure on next page.)

Fig. 4 Minocycline for the treatment of age-related phenotypes in Rp58 hetero-KO mice. **A** Experimental schedule of drug intervention. **B** The effect of minocycline on ssDNA accumulation (a marker of DNA damage) in neurons in the dentate gyrus of *Rp58* hetero-KO mice. $^{*}p < 0.05$, $^{**}p < 0.01$; $n = 4$ for both genotypes with normal water, and $n = 3$ for both genotypes with minocycline. scale bar = 20 µm. **C** The effect of minocycline on gamma-H2AX protein accumulation in neurons in the dentate gyrus of *Rp58* hetero-KO mice. $^{*}p < 0.05$; $n = 3$ per group. scale bar = 20 µm. **D** The effect of minocycline on microglial activation in the dentate gyrus of *Rp58* hetero-KO mice. $^{*}p < 0.05$, $^{**}p < 0.01$; $n = 4$ for both genotypes with normal water, and $n = 3$ for both genotypes with minocycline. scale bar in left = 20 µm, scale bar in right = 10 µm. **E** The effect of minocycline on the impairment of spatial memory in *Rp58* hetero-KO mice. $^{*}p < 0.05$; $n = 8$ for 4–5-month-old wild-type mice with minocycline, and $n = 13$ for 4–5-month-old *Rp58* hetero-KO mice with minocycline. In this figure, the data from Figs. 1 and 2 has been reposted to show the control conditions (normal water)

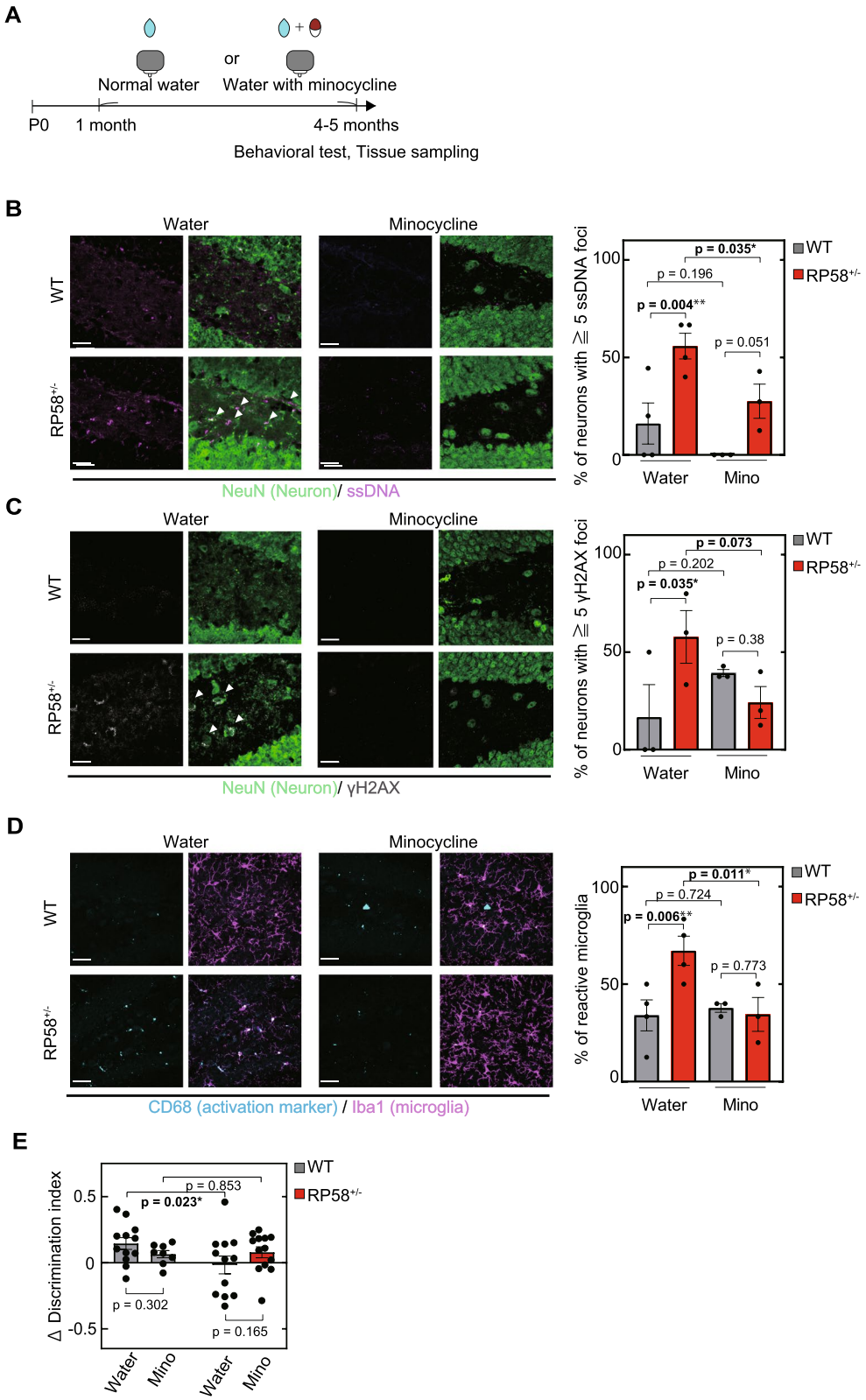

Fig. 4 (See legend on previous page.)

for inflammatory diseases, and clinically, drug repositioning is easier than drug development.

Rp58 hetero-KO mice have the same level of cognitive function as wild-type mice at 2 months, but not at 4–5 months, suggesting that the 4–5-month-old mice may have dementia, an acquired cognitive impairment, as well as ID, an inherent cognitive impairment. Dementia is an established comorbidity in persons with ID [54], and ID itself is an established risk factor for dementia [55]. RP58 expression is markedly reduced in the cerebral cortex of elderly humans [52], suggesting that RP58 expression may be useful as a biomarker for cognitive changes during aging.

Early cognitive decline in *Rp58* hetero-KO mice was associated with impaired DNA repair, and many early aging syndromes, such as Werner syndrome, are known to be caused by mutations in DNA repair-related genes [56]. In the present study, we reported mitochondrial defects in *RP58* hetero-KO mice in adulthood. Nuclear DNA damage is known to spill over into mitochondria, triggering mitochondrial damage and furthermore, this damage increases with aging [57]. These findings are consistent with the idea that reduced expression of RP58 induces cognitive declines that increase with age. Thus, *RP58* hetero-KO mouse may be useful as a model animal to analyze the relationship between ID and dementia.

We should note that we did not observe significant behavioral defects in open field, rotarod, and fear conditioning tests in 4–5 month-old *Rp58* hetero-KO mice, suggesting that not all features of age-associated brain dysfunction are accelerated in these mice. However, *RP58* hetero-KO mice may exhibit other behavioral abnormalities in addition to that of object location memory at different ages. Altogether our findings suggest that RP58 activity-dependent pathways for DNA repair and inhibition of immune system function may be important for the development and maintenance of cognitive function in mammals.

Supplementary Information

The online version contains supplementary material available at https://doi.org/10.1186/s12974-024-03217-1.

Supplementary file 1.

Supplementary file 2.

Acknowledgements
The authors thank Dr. Masataka Kasai for the use of RP58 mutant mice, Dr. Minoru Saitoe, Dr. Nobuhiro Kurabayashi, Dr. Makoto Hashimoto, and Dr. Hideki Miwa for advice on the work presented here, and Kazuki Shiotani and Yuta Tanisumi for their help with the analysis of the electrophysiology data. We would also like to thank Bioedit Ltd (www.bioedit.com) for English language editing.

Author contributions
T.T., S.H. and H.O. designed the research. H.Y. and H.O. supervised the study. T.T. performed and analyzed most experiments. K.E. performed the sample preparation for electron microscopy. Y.N. performed the complementary DNA microarray analysis of gene expression. H.M. assisted with the setup for the electrophysiological experiment. H.S. performed a part of immunostaining and provided additional help with this study and made important suggestions. T.T. generated all figures and tables. T.T. and H.Y. wrote the manuscript. H.O. and J.H. edited the manuscript.

Funding
This work was partially supported by JSPS KAKENHI (18H02537 to HO, 22H02729 to HO, 23K18169 to HO, 17K16408 to TT, 21H05130 to HY, and 21K18231 to HY), by AMED-PRIME program (20gm6110010h0004 to HY), by AMED-FORCE Program (22gm4010019h0001 to HY), by JST-FOREST Program (JPMJFR2150 to HY), by Takeda Science Foundation to SH and by a Research Grant for Public Health Science, The Naito Foundation and Suzuken Memorial Foundation awarded to TT.

Availability of data and materials
No datasets were generated or analysed during the current study.

Declarations

Ethical approval
All experimental procedures were approved by the Animal Experimentation Ethics Committee of the Tokyo Metropolitan Institute of Medical Science (49,040).

Consent for publication
Not applicable.

Competing interests
The authors declare thsat no competing interests.

Received: 27 February 2024 Accepted: 1 September 2024
Published online: 12 October 2024

References

1. Purugganan O. Intellectual disabilities. Pediatr Rev. 2018;39(6):299–309.
2. Vissers LE, Gilissen C, Veltman JA. Genetic studies in intellectual disability and related disorders. Nat Rev Genet. 2016;17(1):9–18.
3. Depienne C, Nava C, Keren B, Heide S, Rastetter A, Passemard S, et al. Genetic and phenotypic dissection of 1q43q44 microdeletion syndrome and neurodevelopmental phenotypes associated with mutations in ZBTB18 and HNRNPU. Hum Genet. 2017;136(4):463–79.
4. Cohen JS, Srivastava S, Farwell Hagman KD, Shinde DN, Huether R, Darcy D, et al. Further evidence that de novo missense and truncating variants in ZBTB18 cause intellectual disability with variable features. Clin Genet. 2017;91(5):697–707.
5. McRae JF, Clayton S, Fitzgerald TW, Kaplanis J, Prigmore E, Rajan D, et al. Prevalence and architecture of de novo mutations in developmental disorders. Nature. 2017;542(7642):433–8.
6. Wang T, Hoekzema K, Vecchio D, Wu H, Sulovari A, Coe BP, et al. Large-scale targeted sequencing identifies risk genes for neurodevelopmental disorders. Nat Commun. 2020;11(1):4932.
7. Okado H. Nervous system regulated by POZ domain Krüppel-like zinc finger (POK) family transcription repressor RP58. Br J Pharmacol. 2021;178(4):813–26.
8. Okado H, Ohtaka-Maruyama C, Sugitani Y, Fukuda Y, Ishida R, Hirai S, et al. The transcriptional repressor RP58 is crucial for cell-division patterning and neuronal survival in the developing cortex. Dev Biol. 2009;331(2):140–51.
9. Ohtaka-Maruyama C, Hirai S, Miwa A, Heng JI, Shitara H, Ishii R, et al. RP58 regulates the multipolar-bipolar transition of newborn neurons in the developing cerebral cortex. Cell Rep. 2013;3(2):458–71.

10. Heng JI, Qu Z, Ohtaka-Maruyama C, Okado H, Kasai M, Castro D, et al. The zinc finger transcription factor RP58 negatively regulates Rnd2 for the control of neuronal migration during cerebral cortical development. Cereb Cortex. 2015;25(3):806–16.
11. Okado H. Regulation of brain development and brain function by the transcriptional repressor RP58. Brain Res. 2019;1705:15–23.
12. Hirai S, Miwa A, Ohtaka-Maruyama C, Kasai M, Okabe S, Hata Y, et al. RP58 controls neuron and astrocyte differentiation by downregulating the expression of Id1-4 genes in the developing cortex. EMBO J. 2012;31(5):1190–202.
13. Ohtaka-Maruyama C, Miwa A, Kawano H, Kasai M, Okado H. Spatial and temporal expression of RP58, a novel zinc finger transcriptional repressor, in mouse brain. J Comp Neurol. 2007;502(6):1098–108.
14. Hirai S, Miwa H, Shimbo H, Nakajima K, Kondo M, Tanaka T, et al. The mouse model of intellectual disability by ZBTB18/RP58 haploinsufficiency shows cognitive dysfunction with synaptic impairment. Mol Psychiatry. 2023;28(6):2370–81.
15. Qing X, Zhang G, Wang ZQ. DNA damage response in neurodevelopment and neuromaintenance. Febs j. 2023;290(13):3300–10.
16. Zhao Y, Simon M, Seluanov A, Gorbunova V. DNA damage and repair in age-related inflammation. Nat Rev Immunol. 2023;23(2):75–89.
17. Kobayashi K, Imagama S, Ohgomori T, Hirano K, Uchimura K, Sakamoto K, et al. Minocycline selectively inhibits M1 polarization of microglia. Cell Death Dis. 2013;4(3): e525.
18. Zhang L, Huang P, Chen H, Tan W, Lu J, Liu W, et al. The inhibitory effect of minocycline on radiation-induced neuronal apoptosis via AMPKα1 signaling-mediated autophagy. Sci Rep. 2017;7(1):16373.
19. Frye CA, Duffy CK, Walf AA. Estrogens and progestins enhance spatial learning of intact and ovariectomized rats in the object placement task. Neurobiol Learn Mem. 2007;88(2):208–16.
20. Paris JJ, Frye CA. Estrous cycle, pregnancy, and parity enhance performance of rats in object recognition or object placement tasks. Reproduction. 2008;136(1):105–15.
21. Tropp J, Markus EJ. Sex differences in the dynamics of cue utilization and exploratory behavior. Behav Brain Res. 2001;119(2):143–54.
22. Tanaka T, Hirai S, Hosokawa M, Saito T, Sakuma H, Saido T, et al. Early-life stress induces the development of Alzheimer's disease pathology via angiopathy. Exp Neurol. 2020;337: 113552.
23. Lu H, Yue J, Meng X, Nickoloff JA, Shen Z. BCCIP regulates homologous recombination by distinct domains and suppresses spontaneous DNA damage. Nucleic Acids Res. 2007;35(21):7160–70.
24. Bialas AR, Presumey J, Das A, van der Poel CE, Lapchak PH, Mesin L, et al. Microglia-dependent synapse loss in type I interferon-mediated lupus. Nature. 2017;546(7659):539–43.
25. Bachstetter AD, Van Eldik LJ, Schmitt FA, Neltner JH, Ighodaro ET, Webster SJ, et al. Disease-related microglia heterogeneity in the hippocampus of Alzheimer's disease, dementia with Lewy bodies, and hippocampal sclerosis of aging. Acta Neuropathol Commun. 2015;3:32.
26. Sisková Z, Page A, O'Connor V, Perry VH. Degenerating synaptic boutons in prion disease: microglia activation without synaptic stripping. Am J Pathol. 2009;175(4):1610–21.
27. Sisková Z, Mahad DJ, Pudney C, Campbell G, Cadogan M, Asuni A, et al. Morphological and functional abnormalities in mitochondria associated with synaptic degeneration in prion disease. Am J Pathol. 2010;177(3):1411–21.
28. Tryon VL, Penner MR, Heide SW, King HO, Larkin J, Mizumori SJY. Hippocampal neural activity reflects the economy of choices during goal-directed navigation. Hippocampus. 2017;27(7):743–58.
29. Houser CR, Peng Z, Wei X, Huang CS, Mody I. Mossy cells in the dorsal and ventral dentate gyrus differ in their patterns of axonal projections. J Neurosci. 2021;41(5):991–1004.
30. Li T, Chen ZJ. The cGAS-cGAMP-STING pathway connects DNA damage to inflammation, senescence, and cancer. J Exp Med. 2018;215(5):1287–99.
31. GoodSmith D, Chen X, Wang C, Kim SH, Song H, Burgalossi A, et al. Spatial representations of granule cells and mossy cells of the dentate gyrus. Neuron. 2017;93(3):677-90.e5.
32. Buckmaster PS, Strowbridge BW, Kunkel DD, Schmiege DL, Schwartzkroin PA. Mossy cell axonal projections to the dentate gyrus molecular layer in the rat hippocampal slice. Hippocampus. 1992;2(4):349–62.
33. Mah LJ, El-Osta A, Karagiannis TC. gammaH2AX: a sensitive molecular marker of DNA damage and repair. Leukemia. 2010;24(4):679–86.
34. Jung EJ, Kim DR. Ectopic expression of H2AX protein promotes TrkA-induced cell death via modulation of TrkA tyrosine-490 phosphorylation and JNK activity upon DNA damage. Biochem Biophys Res Commun. 2011;404(3):841–7.
35. Barzilai A. DNA damage, neuronal and glial cell death and neurodegeneration. Apoptosis. 2010;15(11):1371–81.
36. Bantug GR, Fischer M, Grählert J, Balmer ML, Unterstab G, Develioglu L, et al. Mitochondria-endoplasmic reticulum contact sites function as immunometabolic hubs that orchestrate the rapid recall response of memory CD8(+) T cells. Immunity. 2018;48(3):542-55.e6.
37. Arnoult D, Soares F, Tattoli I, Girardin SE. Mitochondria in innate immunity. EMBO Rep. 2011;12(9):901–10.
38. Minhas PS, Latif-Hernandez A, McReynolds MR, Durairaj AS, Wang Q, Rubin A, et al. Restoring metabolism of myeloid cells reverses cognitive decline in ageing. Nature. 2021;590(7844):122–8.
39. Maynard S, Fang EF, Scheibye-Knudsen M, Croteau DL, Bohr VA. DNA damage, DNA repair, aging, and neurodegeneration. Cold Spring Harb Perspect Med. 2015;5(10):a025130.
40. Hoeijmakers JH. DNA damage, aging, and cancer. N Engl J Med. 2009;361(15):1475–85.
41. Jinde S, Zsiros V, Nakazawa K. Hilar mossy cell circuitry controlling dentate granule cell excitability. Front Neural Circuits. 2013;7:14.
42. Lu Y, Xiao G, Luo W. Minocycline suppresses NLRP3 inflammasome activation in experimental ischemic stroke. NeuroImmunoModulation. 2016;23(4):230–8.
43. Koellhoffer EC, McCullough LD, Ritzel RM. Old maids: aging and its impact on microglia function. Int J Mol Sci. 2017;18(4):769.
44. Zhang L, Chen J, Yang X, Shen C, Huang J, Zhang D, et al. Hepatic Zbtb18 (Zinc Finger and BTB Domain Containing 18) alleviates hepatic steatohepatitis via FXR (Farnesoid X Receptor). Signal Transduct Target Ther. 2024;9(1):20.
45. Raj DD, Jaarsma D, Holtman IR, Olah M, Ferreira FM, Schaafsma W, et al. Priming of microglia in a DNA-repair deficient model of accelerated aging. Neurobiol Aging. 2014;35(9):2147–60.
46. Li S, Lu H, Wang Z, Hu Q, Wang H, Xiang R, et al. ERCC1/XPF is important for repair of DNA double-strand breaks containing secondary structures. iScience. 2019;16:63–78.
47. Liu H, Moura-Alves P, Pei G, Mollenkopf HJ, Hurwitz R, Wu X, et al. cGAS facilitates sensing of extracellular cyclic dinucleotides to activate innate immunity. EMBO Rep. 2019;20(4):e46293.
48. Jo EK, Kim JK, Shin DM, Sasakawa C. Molecular mechanisms regulating NLRP3 inflammasome activation. Cell Mol Immunol. 2016;13(2):148–59.
49. Kita M, Nakae J, Kawano Y, Asahara H, Takemori H, Okado H, et al. Zfp238 regulates the thermogenic program in cooperation with Foxo1. iScience. 2019;12:87–101.
50. Lim JJ, Hyun S. Minocycline treatment improves proteostasis during Drosophila aging via autophagy mediated by FOXO and Hsp70. Biomed Pharmacother. 2022;149: 112803.
51. Xu Y, Sun Q, Yuan F, Dong H, Zhang H, Geng R, et al. RND2 attenuates apoptosis and autophagy in glioblastoma cells by targeting the p38 MAPK signalling pathway. J Exp Clin Cancer Res. 2020;39(1):174.
52. Lu T, Pan Y, Kao SY, Li C, Kohane I, Chan J, et al. Gene regulation and DNA damage in the ageing human brain. Nature. 2004;429(6994):883–91.
53. Barbosa MC, Grosso RA, Fader CM. Hallmarks of aging: an autophagic perspective. Front Endocrinol (Lausanne). 2018;9:790.
54. Cooper S-A. A population-based health survey of maladaptive behaviours associated with dementia in elderly people with learning disabilities. J Intellect Disabil Res. 1997;41(6):481–7.
55. Silverman WP, Zigman WB, Krinsky-McHale SJ, Ryan R, Schupf N. intellectual disability, mild cognitive impairment, and risk for dementia. J Policy Pract Intellect Disabil. 2013;10(3):245–51.
56. Bohr VA. DNA-related pathways defective in human premature aging. ScientificWorldJournal. 2002;2:1216–26.
57. Fang EF, Scheibye-Knudsen M, Chua KF, Mattson MP, Croteau DL, Bohr VA. Nuclear DNA damage signalling to mitochondria in ageing. Nat Rev Mol Cell Biol. 2016;17(5):308–21.

Publisher's Note